Contents lists available at ScienceDirect

Arabian Journal of Chemistry

journal homepage: www.ksu.edu.sa

Synthesis and evaluation of a novel pyridinyl thiazolidine derivative as an antioxidant and corrosion inhibitor for mild steel in acidic environments

Ghada S. Masaret *, Reem Shah

Chemistry Department, College of Sciences, Umm Al-Qura University, Makkah, Saudi Arabia

ARTICLE INFO

Keywords:
(DICPT) inhibitor
DPPH assay
Mild steel (M.STL)
Potentiodynamic polarization test (PDP)
Electrochemical impedance spectroscopy (EIS)
Adsorption isotherm
Surface investigation
Theatrical approaches

ABSTRACT

A new synthesized (Z)-2-((3,5-dichloropyridin-2-yl)imino)thiazolidin-4-one (**DICPT**) was evaluated as an antioxidant and a corrosion inhibitor for mild steel (M.STL) in a 0.5 M HCl solution. The antioxidant activity of newly synthesized **DICPT** was screened using a DPPH assay, and the results showed that **DICPT** has good antioxidant activity. Electrochemical assessments were conducted utilizing potentiodynamic polarization (PDP) and electrochemical impedance spectroscopy (EIS). A new compound, DICPT, was synthesized, and its chemical structure was established and validated through various spectroscopic techniques, including including infrared (FTIR), nuclear magnetic resonance (NMR), and mass spectroscopy. PDP measurements revealed **DICPT** to be a mixed-type inhibitor. Charge transfer resistance (R_{ct}) increased when inhibitor concentrations increased, according to EIS tests. The inhibition efficiency (%I) showed a corresponding rise with increasing inhibitor concentration, peaking at approximately 94.2 % at 3×10^{-5} M. Langmuir's adsorption isotherm was found to govern the preferred adsorption mode of **DICPT** molecules onto the metal surface. UV–visible spectra confirmed the chemical interaction between **DICPT** molecules and the M.STL surface. AFM investigation indicated the formation of a protective layer on the metal surface, shielding it from corrosive environmental factors. Quantum chemical calculations were compared to experimental results to learn more about how corrosion is stopped and how well it works. Our study demonstrates the innovation of **DICPT** as a dual-function compound, offering both antioxidant and corrosion protection properties. This research contributes to the development of effective corrosion inhibitors for industrial applications.

1. Introduction

Metallic corrosion is now considered a significant financial and safety problem in almost all industries in the world. Metals corrode when they come into contact with their environment, such as when acids are used in descaling and acid pickling in the industrial sector (Öztürk, 2017; Alhaffar et al., 2018; Hegazy et al., 2015). Due to this destructive phenomenon, scientists have begun utilizing corrosion inhibitors to mitigate it. For instance, it has been found that the organic compounds act as corrosion inhibitions during acidification in industrial scrubbing procedures (El-Haddad and Fouda, 2015; Rao et al., 2009; Gerengi et al., 2018). These the organic compounds are used as corrosion inhibitors because they include important heteroatoms like O, N, S, etc., which have greater basicity and electron density. This makes them effective for adsorbing onto metal surfaces (El-Haddad and Fouda, 2013; Abdel-Rehim et al., 2006; Lgaz et al., 2020). The presence of lone pairs of heteroatoms (O, N, S, and P) and π-electrons in inhibitor molecules enables the transfer of electrons from the inhibitor to the unoccupied d-orbitals of the metal. This results in the creation of coordinating covalent bonds between the inhibitor molecules and the metal atoms on the surface (El-Haddad and Elattar, 2013; Masroor et al., 2017). The adsorption of inhibitor molecules at the interface between the metal and solution is often affected by factors such as the metal's composition and surface charge, the kind of corrosive electrolyte, and the chemical structure of the inhibitors. Thiazolidine derivatives are eco-friendly molecules that have extensive uses in the food industry, medicinal, and biological sectors, as well as in antioxidant research (Patel et al., 2012; Deep et al., 2016; Wang et al., 2011; Apotrosoaei et al., 2014; Nezhawy et al., 2009; Brahmbhatt et al., 2019; Isloor et al., 2013). Thiazolidine derivatives with extra heteroatoms such as nitrogen (N) and oxygen (O), as well as aryl groups, have been used as corrosion inhibitors for metals in different harsh environments (Alamry et al., 2022; Yadav et al., 2015; Masaret et al., 2021; Keshk and Fouda, 2014; Lgaz et al., 2021; Sehmi et al., 2020; Benali, 1653; Boudjellal et al.,

* Corresponding author: Tel.: +966500063445.
E-mail addresses: gsmasaret@uqu.edu.sa (G.S. Masaret), rkshah@uqu.edu.sa (R. Shah).

https://doi.org/10.1016/j.arabjc.2024.105807
Received 19 March 2024; Accepted 21 April 2024
Available online 22 April 2024

2020; Ouici et al., 2013).

This study focuses on the production of a new compound called (Z)-2-((3,5-dichloropyridin-2-yl)imino)thiazolidin-4-one (**DICPT**), which is a pyridine thiazolidine derivative. We examine its antioxidative characteristics and its ability to suppress corrosion in a 0.5 M HCl solution for M.STL. The chemical structure of **DICPT** was verified using proton nuclear magnetic resonance (^{1}H NMR and ^{13}C NMR), Fourier-transform infrared spectroscopy (FT-IR), and melting point determinations. The antioxidant activity of **DICPT** was shown to be considerable based on the results of the Diphenyl-picrylhydrazyl (**DPPH**) assay, indicating its potential use in the field of medicine. The corrosion inhibition efficacy of **DICPT** for M.STL in a chloride solution was evaluated using potentiodynamic polarization (PDP) and electrochemical impedance spectroscopy(EIS) methods. The metal's surface morphology was analysed using ultraviolet/visible (UV/Vis) spectroscopy and atomic force microscopy (AFM). In addition, density functional theory (DFT) calculations were used to determine the electronic properties and reactivity descriptors of **DICPT**. The obtained results were then compared to experimental data in order to understand the mode, adsorption mechanisms, and interactions of this inhibitor at the metal/solution interface.

In conclusion, our study aims to investigate the effectiveness of this novel Pyridinyl Thiazolidine derivative as both an antioxidant and a corrosion inhibitor for mild steel in acidic environments. By elucidating its properties and performance, we seek to contribute to the understanding of corrosion prevention methods and offer insights into the potential applications of this compound in industrial settings. This research not only addresses a pressing concern in materials science but also opens doors to innovative solutions for corrosion control and antioxidant protection.

2. Materials and experimintal

2.1. Equipments

The determination of the melting point was carried out using a Gallenkamp electric instrument. Infrared spectral data were collected as KBr discs using the ThermoScientific Nicolet IS10 FTIR spectrometer. NMR spectra for ^{1}H and ^{13}C in DMSO-d_6 were acquired using a JEOL spectrometer (500 MHz and 125 MHz, respectively). The mass analysis was acquired with GC–MS equipment (DSQII model), operating at an electron energy of 70 electron volts (eV). Elemental compositions of C, H, and N were analyzed using a Perkin Elmer 2400 analyzer. Antioxidant assesments were conducted employing a UV–visible spectrophotometer (Spekol 11 spectrophotometer, Analytic Jena AG, Jena, Germany) and a UV lamp (Vilber Lourmat-6.LC, VILBER Smart Imaging, Marne-la-Vallée, France). A Gamry Potentiostat/Galvanostat ZRA analyzer (Model: PCI4G750) was used to measure electrochemistry. Surface morphology analysis of M.STL before/after immersion in 0.5 M HCl with/without an inhibitor was conducted using the Nanosurf Flex AFM instrument.

2.2. Chemicals and reagents

3,5-Dichloro-2-chloroacetamido-pyridine (purity: 99 %) and Ammonium Thiocyanate (NH_4SCN) with (purity: 97 %) were procured from Aldrich and utilized without further purification.

All solvents employed in this study were of high-performance liquid chromatography (HPLC) grade, ensuring optimal purity and quality for the experimental procedures.

2.3. Materials and solutons

The chemical composition of mild steel (M.STL) coupons were used for electrochemical measurements and AFM analysis having the following (W%): C (0.17 %), P (0.02 %), Mn (0.472 %), Si (0.25 %). S (0.018 %) and the rest percent is iron. The (M.STL) sheet was cut into a coupon with dimensions of (1.0 cm × 1.0 cm × 0.5 cm) and then embedded in epoxy resin in epoxy resin inside a glass tube. To establish an electrical connection, a copper wire was soldered to the back of the coupon. The exposed surface area of the electrode, which was 0.5 cm^2, underwent abrasion using a series of emery papers up to a 1200 grade level. Following this, the electrode was rinsed with distilled water and ethanol to eliminate any potential residue from the polishing process. Finally, it was air dried and employed as the working electrode in the electrochemical methods (Fouda et al., 2008). The corrosive HCl solution (0.5 M) was prepared by by dilution of analytical grade 37 % HCl with deionized water. The concentration range of investigated (DICPT) inhibitor was ($1 \times 10^{-5} - 3.0 \times 10^{-5}$ M) were prepared by suitable dilution in 0.5 M HCl.

2.4. Synthesis of 2-((3,5-dichloropyridin-2-yl)imino)thiazolidin-4-one (DICPT)

A mixture of 3,5-dichloro-2-chloroacetamido-pyridine (**DICAP**) (0.96 g, 4 mmol) and NH_4SCN (0.38 g, 5 mmol) was refluxed in ethyl alcohol (30 mL) for 4 h. The reaction mixture was then cooled to room temperature. The solid product (**DICPT**) was filtered using Whatman filter paper No. 1 (Whatman Int. Ltd., Kent, UK) and washed with cold ethanol (10 mL). The solid that obtained was purified by crystallization from ethanol to furnish the targeting pyridinyl thiazolidine derivative with retention factor ($R_f = 0.41$) using eluent from petroleum ether and ethyl acetate (1:1). Yellowish green solid, yield = 72.6 %, m.p. = 286–287 °C. IR (ν/cm^{-1}): 3161 (N–H), 1721 (C = O). ^{1}H NMR (DMSO-d_6): 3.91 (s, 2H, CH_2), 8.07 (d, J = 2.50 Hz, 1H, pyridine-H_4), 8.67 (d, J = 2.50 Hz, 1H, pyridine-H_6), 12.05 ppm (s, 1H, N–H). ^{13}C NMR (DMSO-d_6): 34.17, 121.66, 124.03, 140.38, 145.59, 156.51, 163.92, 172.43. Mass analysis, m/z = 261.86 (16.08 %) (Fig. S2). Analysis of $C_8H_5Cl_2N_3OS$ (260.95): Calculated: C, 36.66; H, 1.92; N, 16.03 %. Found: C, 36.83; H, 2.00; N, 15.91 %.

2.5. Antioxidant activity using DPPH assay

In this study,-Diphenyl-picrylhydrazyl (DPPH$^{\bullet}$) and DMSO solvent were acquired from Sigma Aldrich and used throughout the antioxidant activity studies. The antioxidant capacity of the **DICPT** derivative was evaluated using the DPPH technique. Ascorbic acid served as the reference standard. The methodology followed a previously reported approach (Kitts et al., 2000). Serial dilutions of the tested samples were prepared in methanol. A 0.135 mM solution of DPPH was then mixed with each dilution in equal volumes. After incubation for 30 min, the sample absorbance was evaluated at λ_{max} (517 nm). The % of remaining DPPH was deliberated using the ensuing equation:

$$\%DPPH_{\text{Remaining}} = \left[\frac{Control_{abs}}{Sample_{abs}}\right] \times 100 \quad (1)$$

where $Control_{abs}$ is the absorbance of blank at t = 0 min; and $Sample_{abs}$ is the absorbance of the antioxidant at t = 30 min.

The outstanding DPPH was planned against sample's concentration (mg/mL) using an exponential curve to determine the IC_{50} value. The IC_{50} represents the sample's concentration compulsory to unhibit 50 % of the DPPH radical concentration. Lower IC_{50} values indicate stronger antioxidant capacity. This approach aligns with the established principle that a sample with a higher antioxidant capacity will have a lower IC_{50} value.

2.6. Electrochemical method

As previously mentioned, electrochemical investigations have been conducted using a typical three electrode electrochemical glass-cell, which involves the working electrode (M.STL), a counter electrode (Pt foil), and a reference electrode (saturated calomel electrode; SCE) (El-

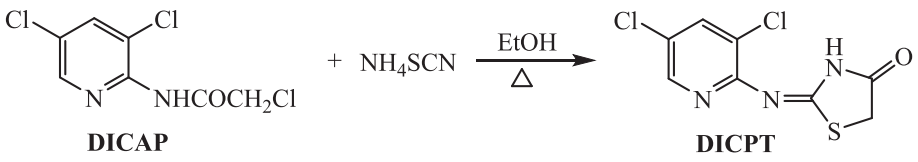

Fig. 1. Synthesis of DICPT.

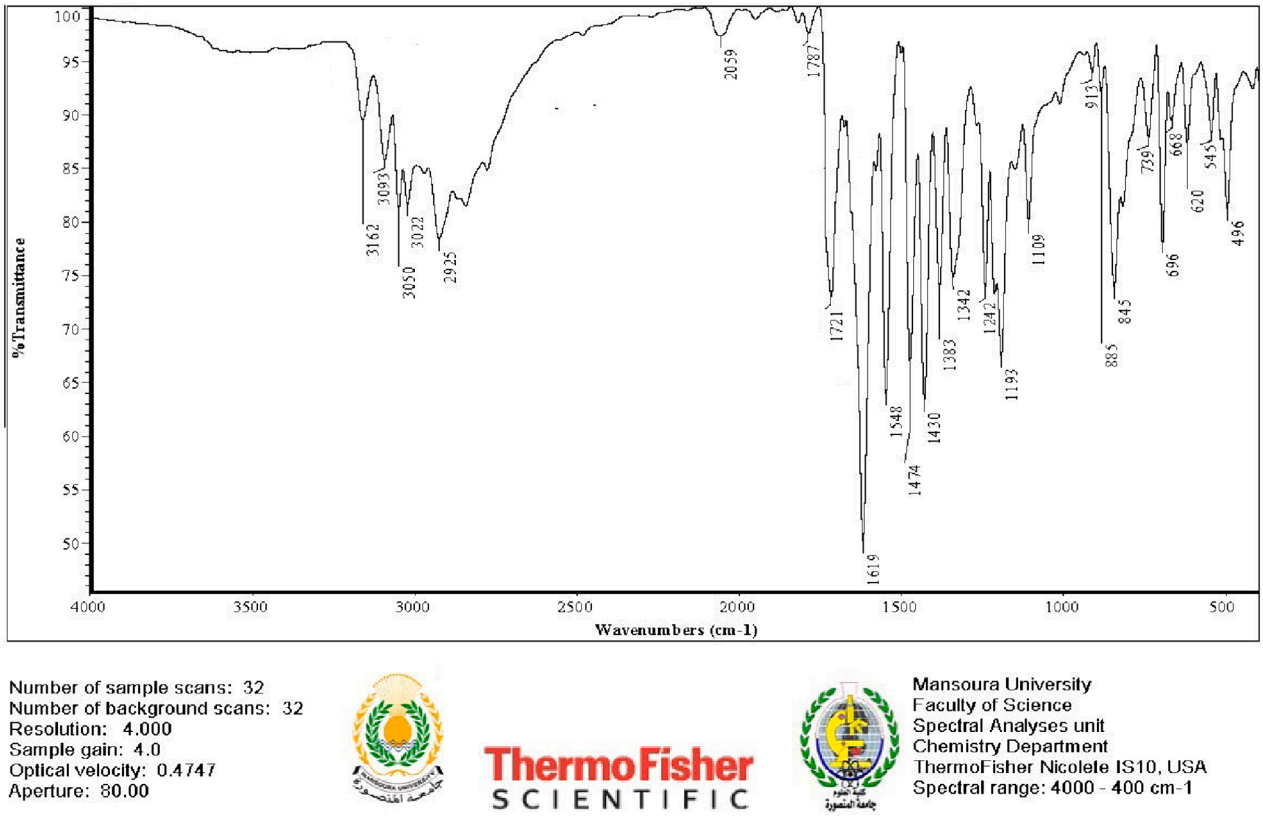

Fig. 2. The FTIR spectrum of **DICPT**.

Haddad et al., 2013). The working electrode (M.STL) was interleaved into the test solution for 45 min, in oder to chieve the open circuit potential (OCP). In the potentiodynamic polarization (PDP) test the current–potential curves were generated by varying the electrode potential within the range of (−250 to + 250 mV) at a scan rate of (0.1 mV/s). All potentials are expressed in millivolts (SCE). The electrochemical impedance spectroscopy (EIS) experiment was conducted at (OCP) across a frequency spectrum ranging from (100 kHz to 20 mHz). A sinusoidal potential perturbation of (5.0 mV) in amplitude was applied. A Gamry Potentiostat/Galvanostat ZRA analyzer (Model: PCI4G750, Germeny) was used to record electrochemical measuremnts.

2.7. UV–visible spectroscopy

UV–visible spectra measurements were obtained using a PG instrument (T80 + UV/vis spectrometer, UK) with a double-beam operated at a bandwidth of 1.0 nm (190–1100 nm). The spectra were measured on the **DICPT** solution before and after immersing M.STL in the test solution at room temperature for 48 h (Abdou and El-Haddad, 2022).

2.8. Atomic force microscopy (AFM) surface analysis

In preparation for the morphology study, the M.STL samples were dipped in corrosive solutions at room temperature for 48 hrs., then the samples were removed, rinsed with deionized H_2O, and then dried (Hilbert et al., 2003). The properties of the protecting layer of (**DICPT**) designed on the M.STL surface were investigated using AFM (N9498S Agilent Technologies) analysis.

2.9. Theatrical calculations

Quantum chemical calculations for (**DICPT**) were applied in a queuing phase using the theotheical method (DFT)., using the Gaussian program (version 9.0, USA). Meanwhile, both of (E_{HOMO}), (E_{LUMO}), and other derived amounts were determined and visualized utilizing Gauss View 3.0. (El-Haddad, 2020).

3. Results and discussion

3.1. Synthesis of DICPT

A solution containing 3,5-dichloro-2-chloroacetamido-pyridine (DICAP) (0.96 g, 4 mmol) and NH_4SCN (0.38 g, 5 mmol) was refluxed in ethyl alcohol (30 mL) for 4 h (Al-nami et al., 2021). Upon cooling, the resulting solid was filtered to isolate the target pyridine-thiazolidin-4-one hybrid (DICPT) (as shown in Fig. 1).

The obtained product exhibited physical properties of a yellowish-green solid with a yield of 72.6 % and a melting point recorded at

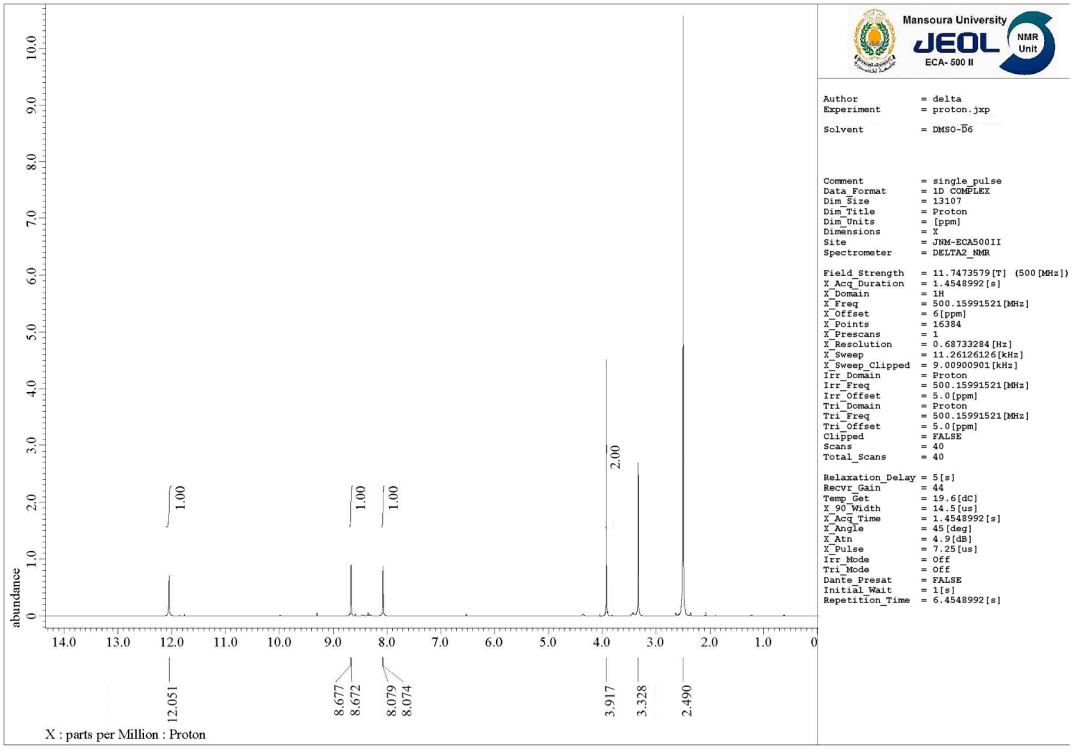

Fig. 3. The ^{1}H NMR (DMSO-d_6) spectrum of **DICPT**.

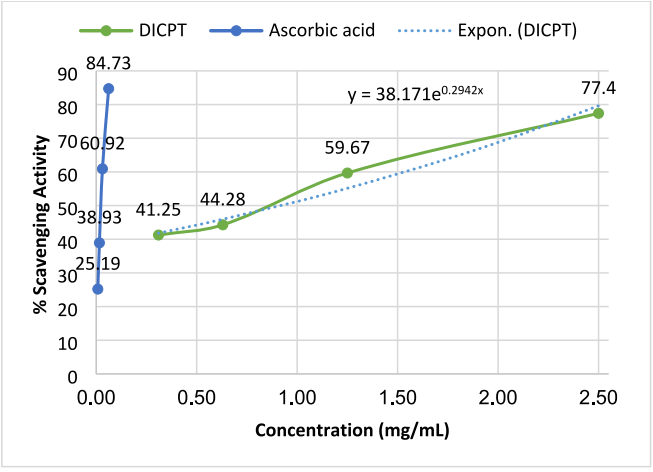

Fig. 4. A relation between the sample concentration (mg/mL) versus % scavenging activity.

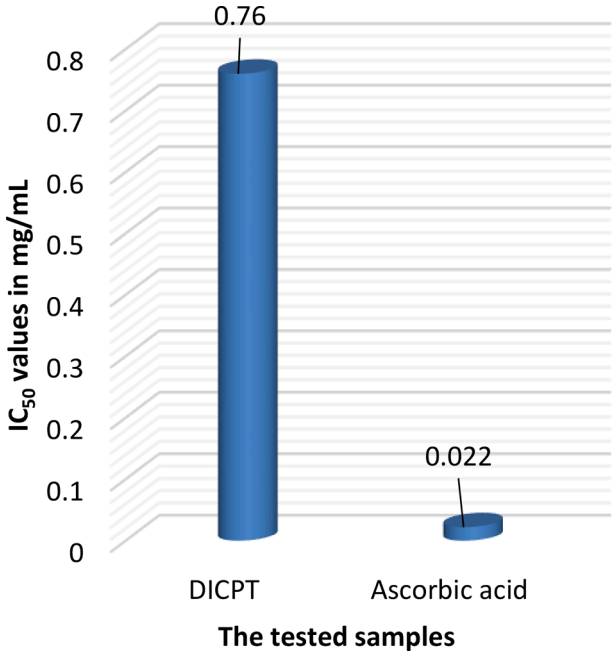

Fig. 5. Comparison of the IC_{50} values of the investigated samples.

286–287 °C.

This synthesized **DICPT** was further characterized by infrared (FTIR) spectroscopy, revealing characteristic absorption peaks at 3161 cm^{-1}and 1721 cm^{-1}, respectively, corresponding to (N–H) and (C = O) group group within the thiazolidin-4-one ring (as shown in Fig. 2).

Further elucidation of the compound's structure was achieved through (^{1}H NMR) spectroscopy, conducted in (DMSO-d_6). The ^{1}H NMR spectrum exhibited distinctive resonances, with the methylene protons appearing as a singlet at δ 3.91 ppm. The pyridine protons were observed as doublets at δ 8.07 ppm (pyridine-H4) and doublets of doublets at δ 8.67 ppm (pyridine-H6). Additionally, a singlet peak was observed at δ 12.05 ppm, corresponding to the NH group proton (as shown in Fig. 3).

In addition, the analysis of ^{13}C NMR spectrum (Fig. S1) in DMSO-d_6 solvent showed characteristic peaks at 34.17, 121.66, 124.03, 140.38, 145.59, 156.51, 163.92, and 172.43 ppm, further supporting the structural elucidation.

The elemental analysis of the **DICPT**, calculated for the molecular formula $C_8H_5Cl_2N_3OS$ (260.95): Calculated: C, 36.66; H, 1.92; N, 16.03 %., closely matched the experimental findings (Found: C, 36.83; H, 2.00; N, 15.91 %). These results corroborate the successful synthesis and characterization of the DICPT compound.

3.2. Antioxidant activity of DICPT

Based on the obtained data (Table S1 and Figs. 4 and 5**),** compound **DICPT** exhibits concentration-dependent antioxidant activity, as evidenced by the increasing percentage of DPPH radical scavenging activity with increasing concentration. At the highest concentration tested (2.5 mg/mL), **DICPT** demonstrated an average scavenging activity of 77.40 ± 1.46 %. This suggests that doubling the concentration of **DICPT** could potentially lead to a 20 % increase in its scavenging activity. Ascorbic acid, included as a reference standard, exhibited significantly higher antioxidant activity than compound **DICPT** at all concentrations tested. This is evident by the consistently higher percentage of DPPH scavenging activity and lower IC_{50} values for ascorbic acid. For instance, at the lowest concentration tested (0.008 mg/mL), ascorbic acid exhibited a scavenging activity of 25.19 ± 0.96 %, while data for DICPT was not available at this concentration. The significantly lower IC_{50} value of ascorbic acid (0.022 ± 0.58 mg/mL) compared to compound **DICPT** (0.76 ± 0.03 mg/mL) further supports this finding. This means that a lot less ascorbic acid is needed to get rid of 50 % of the DPPH radicals, indicating its stronger antioxidant capacity compared to **DICPT**.

The IC_{50} value, which is the concentration needed to scavenge 50 % of the DPPH radicals, for DICPT is 0.76 ± 0.03 mg/mL. A lower IC_{50} value indicates a stronger antioxidant capacity, meaning less of the compound is needed to scavenge 50 % of the DPPH radicals. This value is based on data from all four concentrations that were tested: 2.5 mg/mL, 1.25 mg/mL, 0.63 mg/mL, and 0.31 mg/mL. Generally, the results suggest that compound **DICPT** possesses antioxidant activity, but to a lesser extent compared to ascorbic acid. The fact that the response changed with concentration and the IC_{50} value was lower at the highest concentration tested suggests that compound **DICPT** may need to be at higher concentrations to have the same antioxidant effect as ascorbic acid. The significantly lower IC_{50} value of ascorbic acid (0.022 ± 0.58 mg/mL) compared to compound **DICPT** (0.76 ± 0.03 mg/mL) still holds true. This means that a lot less ascorbic acid is needed to get rid of 50 % of the DPPH radicals. This suggests that ascorbic acid is a better antioxidant overall based on this test. This observation aligns well with the overall results, where ascorbic acid exhibited consistently higher scavenging activity at all concentrations tested. The significantly lower IC_{50} value of ascorbic acid (0.022 ± 0.58 mg/mL) compared to DICPT (0.76 ± 0.03 mg/mL) further supports this finding. Thus, the IC_{50} value provides valuable information about the antioxidant potential of **DICPT** at the tested concentrations.

To elucidate the mechanistic underpinnings of **DICPT's** antioxidant activity observed in the DPPH assay, we will now explore the structure–activity relationship (SAR) of this molecule. Specifically, we will investigate how the positioning and electronic properties of its functional groups (imine, secondary amine, and carbonyl) might influence their propensity to engage in hydrogen atom transfer (HAT), single electron transfer (SET), or chelation with the DPPH radical. **DICPT** has an imine group (C = N) that may help it be an antioxidant through hydrogen atom transfer (HAT) (Capaldo and Ravelli, 2017) or single electron transfer (SET) (Plesniak et al., 2017). The nitrogen atom in the imine can donate an electron, which could make it easier for a hydrogen atom (Chen et al., 2020) or an electron to be given to the DPPH radical (Foti, 2015), which would stop it from working. The secondary amine (NH) group might be able to donate a hydrogen bond to the DPPH radical, interacting with it and changing how stable it is (Balachandar, 2017). However, the overall impact of this interaction on scavenging activity is unclear and might depend on the specific positioning of the NH group within the molecule. The carbonyl group (C = O) in the thiazolidinone ring might participate in chelation with the DPPH radical (Adjimani and Asare, 2015). The carbonyl group can give the carbon next to it a positive charge by taking electrons away. This makes the adjacent carbon more attractive to the lone pair electrons on the oxygen atom of the DPPH radical. However, the chelation process might not work as well depending on where the carbonyl group is in relation to the imine and how much space there is in the molecule.

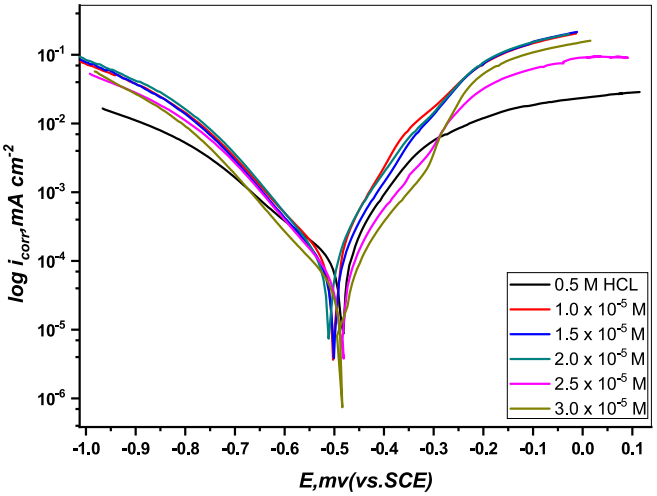

Fig. 6. PDP plots of **M.STL** in test solution with/without (**DICPT**) concentrations.

The proposed mechanisms for DICPT's antioxidant activity involve either hydrogen atom transfer (HAT) or single electron transfer (SET) to the DPPH radical. In the HAT mechanism, a hydrogen atom from DICPT (represented as R-NH-C = N-R') is transferred to the DPPH radical, forming a stable DICPT radical and a non-radicalized form of DPPH (hydrazine). The 'R' and 'R'' represent substituent groups on the DICPT molecule. Alternatively, the SET mechanism proposes the transfer of a single electron from DICPT to the DPPH radical. This creates a positively charged **DICPT** radical cation (**DICPT**$^{+}$) and a negatively charged DPPH anion (DPPH^{-}). Both mechanisms offer potential pathways for **DICPT** to scavenge free radicals, potentially contributing to its observed antioxidant activity.

R-NH-C = N-R' (DICPT) + DPPH → R-NH-C = N-R'' + DPPH-H.

where, R and R' represent substituents on the molecule.

R-NH-C = N-R' (DICPT) + DPPH → R-NH-C = N-R'$^{+}$ + DPPH^{-}.

These are simplified representations, and the actual mechanism might involve a combination of factors like bond dissociation energies, resonance stabilization, and solvent effects. Additionally, the specific functional groups involved (imine, NH, and carbonyl) can influence the favored mechanism (HAT vs. SET) but require further investigation for compound **DICPT**.

The proposed mechanisms suggest that **DICPT** has the potential for antioxidant activity, but the effectiveness might be lower compared to ascorbic acid. **DICPT** relies on specific functional group positioning and nearby hydrogens for optimal activity in HAT or SET mechanisms. Ascorbic acid, on the other hand, utilizes diverse mechanisms, including direct hydrogen atom donation from its enol form. This versatility and ease of hydrogen donation likely contribute to ascorbic acid's superior performance observed in the lower IC_{50} value achieved with a much lower concentration compared to **DICPT**.

The DPPH assay serves as a useful initial screening method for antioxidant activity. While complex reactions beyond free radical scavenging are often involved in corrosion mechanisms, the ability to scavenge free radicals can be advantageous for a corrosion inhibitor. During the corrosion process, free radicals can contribute to the breakdown of the protective passive layer on the metal surface. Antioxidants like DICPT have the potential to scavenge these free radicals, potentially leading to a slower corrosion rate. It's important to note that the DPPH assay provides a starting point, and further studies are needed to fully understand the mechanism by which DICPT might influence corrosion inhibition.

Table 1
The corrosion parameters obtained from potentiodynamic polarization (PDP) analysis.

Conc., M	i_{corr}, μA cm^{-2}	$-E_{corr}$, mV	B_a, mV dec^{-1}	B_c, mV dec^{-1}	θ	$\%I_{PDP}$
0.5 M HCl	756	310	97	164	–	–
1.0×10^{-5}	235.8	341	99	140	0.668	66.5
1.5×10^{-5}	199.5	345	103	136	0.736	73.6
2.0×10^{-5}	146.6	357	107	131	0.806	80.6
2.5×10^{-5}	94.50	365	113	126	0.875	87.5
3.0×10^{-5}	42.33	401	117	121	0.944	94.4

3.3. Electrochemical studies

3.3.1. Potentiodynamic polarization (PDP) tests

Fig. 6 shows the PDP curves of M.STL in a 0.5 M HCl solution with and without various **DICPT** concentrations at 30 °C. Two branches can be seen in the polarization curves, which represent the anodic Fe oxidation and cathodic hydrogen ion reduction processes.

The data provides insights into how the presence of DICPT influences these electrochemical reactions, shedding light on the corrosion behavior of the metal in acidic solutions.

An analysis of the polarization curves obtained in the uninhibited acid solution and the inhibited acid solutions (**DICPT**) reveals a slight shift in the corrosion potential towards the anodic direction. In addition, the anodic and cathodic current densities shift to lower values in the inhibited curves. It has been observed that this effect depends on the concentration of the **DICPT**; the effect was greatest at the highest examined concentration. This indicates that (**DICPT**) has high inhibiting properties that are enhanced by increasing inhibitor concentration.

It appears that the corrosion potential was slightly shifted in an anodic direction suggests that (**DICPT**) behaves as a mixed type corrosion inhibitor in 0.5 M HCl solution (Abdelaziz et al., 2021), but with a greater impact on the anodic processes.

Table 1 presents the PDP parameters that were obtained from the analysis of the potentiodynamic curves. The i_{corr} measurements were applied to calculate the inhibition efficiency ($\%I_{PDP}$) and surface coverage (θ) using the formula (El Haddad Mahmoud et al., 2023):

$$\%\boldsymbol{I_{PDP}} = \left(\frac{\boldsymbol{i^b_{corr}} - \boldsymbol{i^i_{corr}}}{\boldsymbol{i^i_{corr}}}\right) \times 100 \tag{2}$$

$$\boldsymbol{\theta} = \left(\frac{\boldsymbol{i^b_{corr}} - \boldsymbol{i^i_{corr}}}{\boldsymbol{i^i_{corr}}}\right) \tag{3}$$

where, i^b_{corr} and i^i_{corr} are the current density without/with (**DICPT**), respectively.

The i_{corr} values of the inhibited solutions are lower than that of the blank (0.5 M HCl) solution, as expected. Furthermore, as the concentration of **DICPT** increases, the icorr values further decline. This signifies an improvement in corrosion inhibition efficiency to 94.4 % (Table 1). The β_a and β_c values are used to characterize the anodic and cathodic polarization behavior, respectively. It's noted that with an increase in inhibitor concentration, the β_a value increases, indicating a shift towards more positive potentials for anodic reactions. However, the β_c value remains unchanged with varying **DICPT** concentration, suggesting that the mechanism of cathodic reactions remains unaffected (Gerengi et al., 2018). The increase in β_a value with increasing **DICPT** concentration suggests that adsorbed **DICPT** molecules may be influencing the mechanism of anodic reactions. This indicates that **DICPT** molecules likely adsorb onto the surface of M.STL, forming a protective layer that impedes the dissolution of the steel in the aggressive HCl medium. In summary, the effectiveness of **DICPT** as a corrosion inhibitor for M.STL in acidic environments, attributing its inhibitive properties to the formation of an adsorbed film that protects the steel surface from corrosion.

3.3.2. Electrochemical impedance spectroscopy (EIS) tests

Impedance measurements were performed to evaluate the protection ability of the synthesized (**DICPT**) for (**M.STL**) in the corrosive medium. Fig. 7 displays the Nyquist (a) and Bode (b and c) graphs of (**M.STL**) dipped in 0.5 M HCl solution with/without (**DICPT**) at 30C. As shown by the appearance of a single capacitive loop at high frequency (Fig. 7a), the charge transfer at the electrode/solution interface controls (**M.STL**) dissolution in test solution. It has been noted that both inhibited and uninhibited systems maintain the general form of the Nyquist curve. This implies that the corrosion mechanism is unaffected by the addition of (**DICPT**).

Bode and phase angle charts are displayed in (Fig. 7b–c) indicates that phase angle values rose in the intermediate frequency region as the (**DICPT**) concentration increased relative to the blank solution. This is because a protective (DICPT) inhibitive film was established, enhancing the protective properties of steel (Singh et al., 2023).

Additionally, for Bode plots the values of impedance rise with the rising **DICPT** amount in the lower region of frequency which is an indication of the **DICPT** adsorption and prevention of steel corrosion (Singh et al., 2023). The circuit was used for analysis of the EIS data is publushid prevouisly (El-Haddad et al., 2021). In this circuit, R_s, R_{ct}, and (C_{dl}) are the solution resistance, charge-transfer resistance and a double layer capacitor, respectively.

Table 2 summarizes the electrochemical parameters derived from the impedance procedure. The ($\%I_{EIS}$)and (θ) were obtained according to the flolowing equation (Dohare et al., 2017):

$$\%\boldsymbol{I_{EIS}} = \left(\frac{\boldsymbol{R^i_{ct}} - \boldsymbol{R^b_{ct}}}{\boldsymbol{R^i_{ct}}}\right) \times 100 \tag{4}$$

$$\boldsymbol{\theta} = \left(\frac{\boldsymbol{R^i_{ct}} - \boldsymbol{R^b_{ct}}}{\boldsymbol{R^i_{ct}}}\right) \tag{5}$$

where, R^i_{ct} and R^b_{ct} are the charge-transfer resistance of (**DICPT**) and 0.5 M HCl, respectively.

The results presented in Table 2 illustrate a clear trend: as the concentration of **DICPT** increases, there is a decrease in the double layer capacity (C_{dl}) value, accompanied by an increase in the charge transfer resistance (R_{ct}) value. This observation suggests an enhancement in the efficiency of the inhibition process. The decrease in (C_{dl}) with increasing **DICPT** concentration may indicate a thickening of the electrical double layer or a reduction in the local dielectric constant.

Moreover, previous studies have indicated that the increase in **DICPT** concentration leads to the formation of an adsorbed film on the metal surface. This film serves as a protective barrier, reducing metal corrosion in acidic solutions and consequently elevating the (R_{ct}) value. Therefore, the rise in (R_{ct}) value is attributed to the formation of this adsorbed film (Hu et al., 2017; Sharma et al., 2023; Thakur et al., 2023; Sharma et al., 2023; Kaya et al., 2023; Thakur et al., 2024).

It is conclude to report that the values of $\%I_{EIS}$ obtained from EIS tests are agreement with obtained by PDP test, supporting the efficacy of **DICPT** as a corrosion inhibitor. This correlation underscores the reliability and consistency of the experimental results across different corrosion testing methods.

3.4. Adsorption isotherm parameters

The interaction type between (**DICPT**) molecules and (M.STL) surface in a 0.5 M HCl solution can be assumed from the adsorption isotherm. To establish this isotherm, we need to determine the fractional surface coverage values (θ) in relation to the inhibitor concentration. These θ values can be easily calculated from Potentiodynamic Polarization (PDP) studies using the inhibition efficiency ratio divided by 100. Therefore, empirical investigation is necessary to identify the most suitable isotherm for describing inhibitor adsorption on M.STL surfaces. Several adsorption models, including Langmuir, Frumkin, Freundlich,

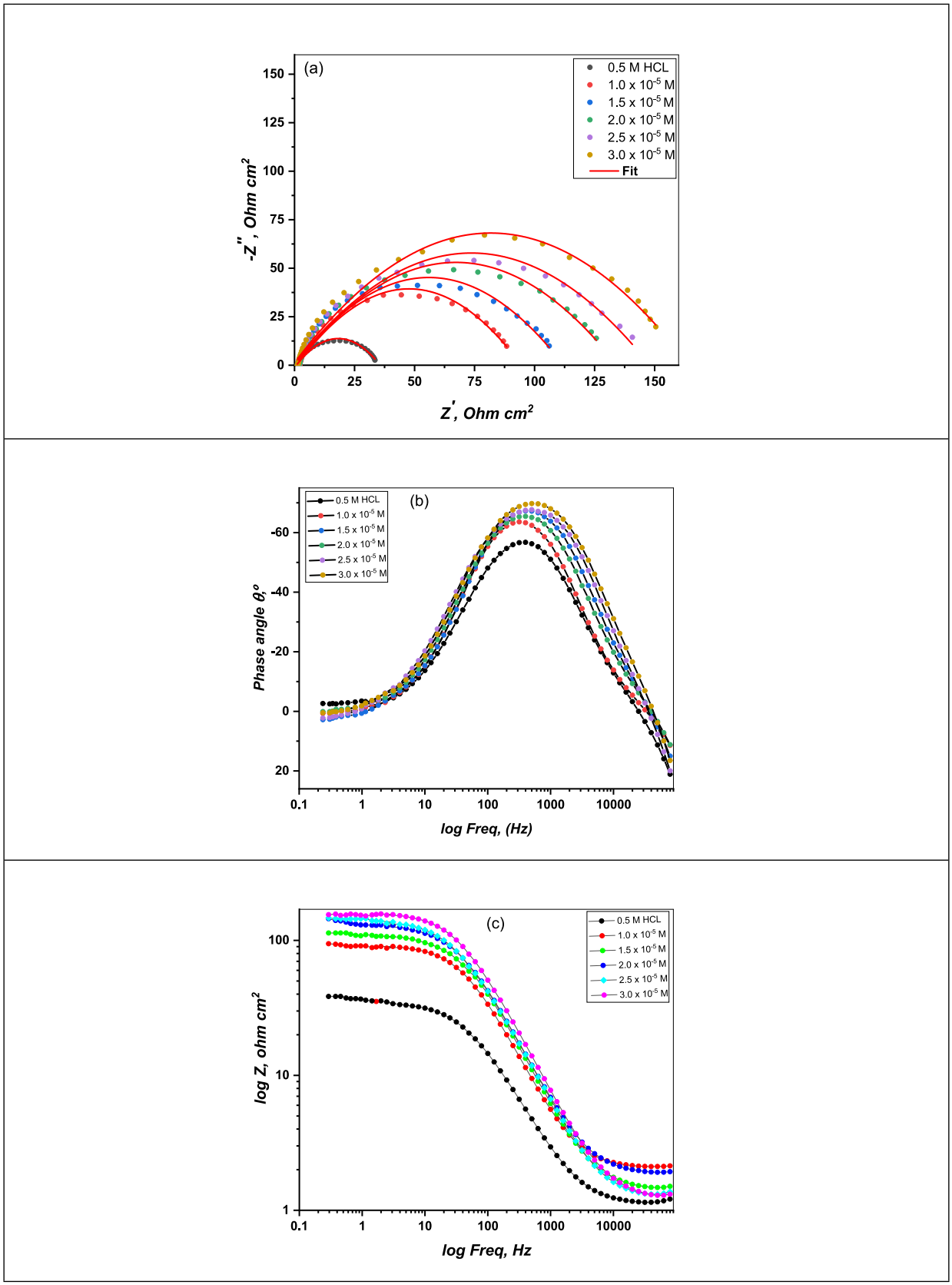

Fig. 7. Nyquist plots (a), Bode plots (b) and Phase angle plots (c) of **M.STL** in test solution with/without (**DICPT**) concentrations.

Table 2
The corrosion parameters of **M.STL** obtained from Impedance Spectroscopy(EIS) analysis.

Conc., M	Rs (Ω cm^2)	R_{ct}, (Ω cm^2)	C_{dl}, (μF cm^{-2})	θ	$\%I_{EIS}$
0.5 M HCl	2.25	34.32	105.3	–	–
1.0×10^{-5}	2.74	109.3	45.7	0.686	68.6
1.5×10^{-5}	2.84	135.2	27.3	0.746	74.6
2.0×10^{-5}	3.02	180.8	30.2	0.810	81.0
2.5×10^{-5}	3.12	291.3	22.7	0.882	88.2
3.0×10^{-5}	3.22	585.5	27.6	0.941	94.1

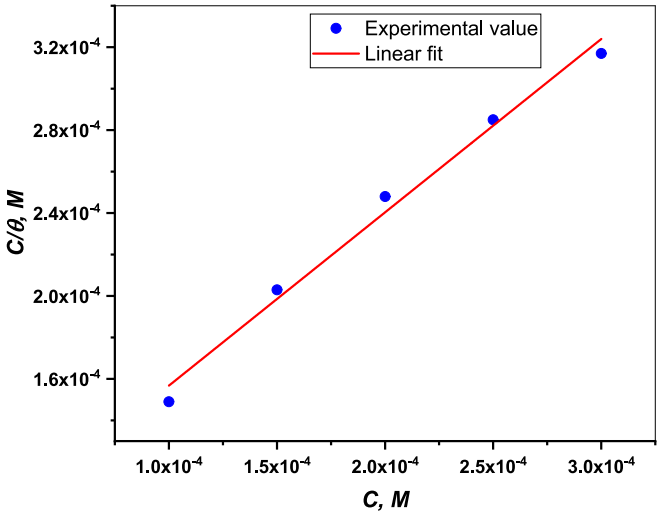

Fig. 8. Langmuir adsorption isotherm of (**DICPT**) on the (M.STL) surface.

and Temkin isotherms, were evaluated. After testing different models, the Langmuir isotherm emerged as the most appropriate choice based on its high correlation coefficient (R^2) values, which were very close to unity. This finding confirms that the adsorption of (**DICPT**) on M.STL in 0.5 M HCl conforms to the Langmuir isotherm model. The Langmuir isotherm model is expressed by the following equation (Ismail et al., 2022):

$$C_i = \frac{C_i}{\theta} - \frac{1}{K_{ads}} \tag{6}$$

where C_i is (**DICPT**) concentration, and K_{ads} is the equilibrium constant of adsorption process.

Fig. 8 displays a straight line on the graph of log (C_i/θ) versus C_i. The linear regression coefficients (R^2) are close to 0.999 for the (**DICPT**) inhibitor. This suggests that the examined (**DICPT**) inhibitor follow Langmuir's adsorption isotherm during adsorption in a 0.5 M HCl solution.

The K_{ads} value obtained from the intercept of the linear (Fig. 8**)** is high value (13.661 $\times$ 10^3 mol/L), indicating the strong adsorption of (**DICPT**) molecules on the (M.STL) surface. The K_{ads} value was applied to determine the free energy of adsorption ($\Delta G^{\circ}a_{ds}$) as follows (Ismail et al., 2022):

$$K_{ads} = \frac{1}{55.5} e\left(-\frac{\Delta G^{\circ}_{ads}}{RT}\right) \tag{7}$$

where the concentration of H_2O inthe solution is 55.5 mol/L, the absolute temperature is T, and R is the universal gas constant. The negative value of (ΔG°_{ads}), indicating that the process is spontaneous. In addition, the value of (ΔG^{o}_{ads}) obtained for (**DICPT**)inhibitor in the current work is (−34.11 kJ/mol), revealing the absorption of (**DICPT**) molecules on the (M.STL) surface is a mixed between (physical and chemical adsorption),

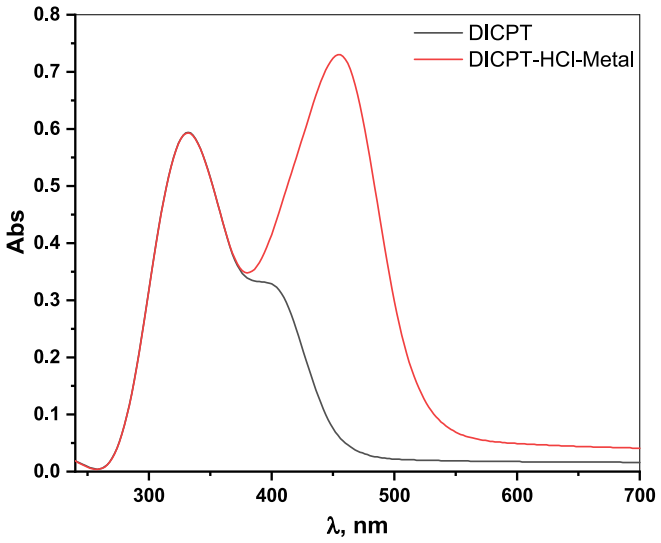

Fig. 9. UV spectra of (**DICPT**) (black color), 1.0 M HCl solution with (**DICPT**) after M.STL immersion (red color) for 48 hrs.

but, there are more physical interactions between the (**DICPT**) molecules and the metal surface (Ismail et al., 2022).

3.5. Spectroscopic measurement (UV–Vis spectroscopy)

The UV–visible spectroscopy tool was employed to investigate how inhibitor molecules interacted with the metal in the test solution. In this study, spectral analysis was conducted both before and after the corrosion test to assess any changes in the system. Fig. 9 presents the UV–VIS spectra of the (**DICPT**) inhibitor solution and the test solution containing (**DICPT**) inhibitor after immersing the M.STL sample for 48 h. In the (**DICPT**) inhibitor solution, distinct absorption peaks were observed at 332 nm and 399 nm. These peaks are attributed to $\pi - \pi^*$ and n-π^* transitions, respectively, associated with the conjugated C = C bonds of the aromatic rings, NH, C = O, and C = N as shown in (Fig. 9, black color). However, in the spectra (Fig. 9, red color), we notice new peak at 454 nm. This suggests an enhanced adsorption of the (**DICPT**) inhibitor on the metal surface, likely due to the formation of π–d bonds. These bonds arise from the overlap of π-electrons with the 3d vacant orbital of Fe atoms. Such behavior is attributed to the presence of N, O atoms, and conjugated double bonds in the (**DICPT**) structure (Bandeira et al., 2017).

3.6. Surface analysis (AFM) spectroscopy

The 2D, 3D AFM pictures and consistent altitude profile plot of (M. STL) surface in 0.5 M HCl solution, and after 48 hrs dipping are represented in Fig. 10.

Furthermore, the morphology of the (free M.STL) was homogeneous and smooth and surface (Fig. 10a), and the corresponding average surface roughness (R_a) value was 17.13 nm. While, the (M.STL) surface is more damaged after immersion in test solution, and the corresponding (R_a) value was 80.23 nm (Fig. 10b), due to the (M.STL)/acid direct interaction.

On the other hand, the (M.STL) surface in test solution (**DICPT**) inhibitor showed that the surface has become more smoother and the corresponding (R_a) value was 32.37 nm (Fig. 10c). This occurs as a result of a shielding layer covering the (M.STL) surface that prevents the direct contact between the acid and steel (Jahdaly and Badreah, 2023).

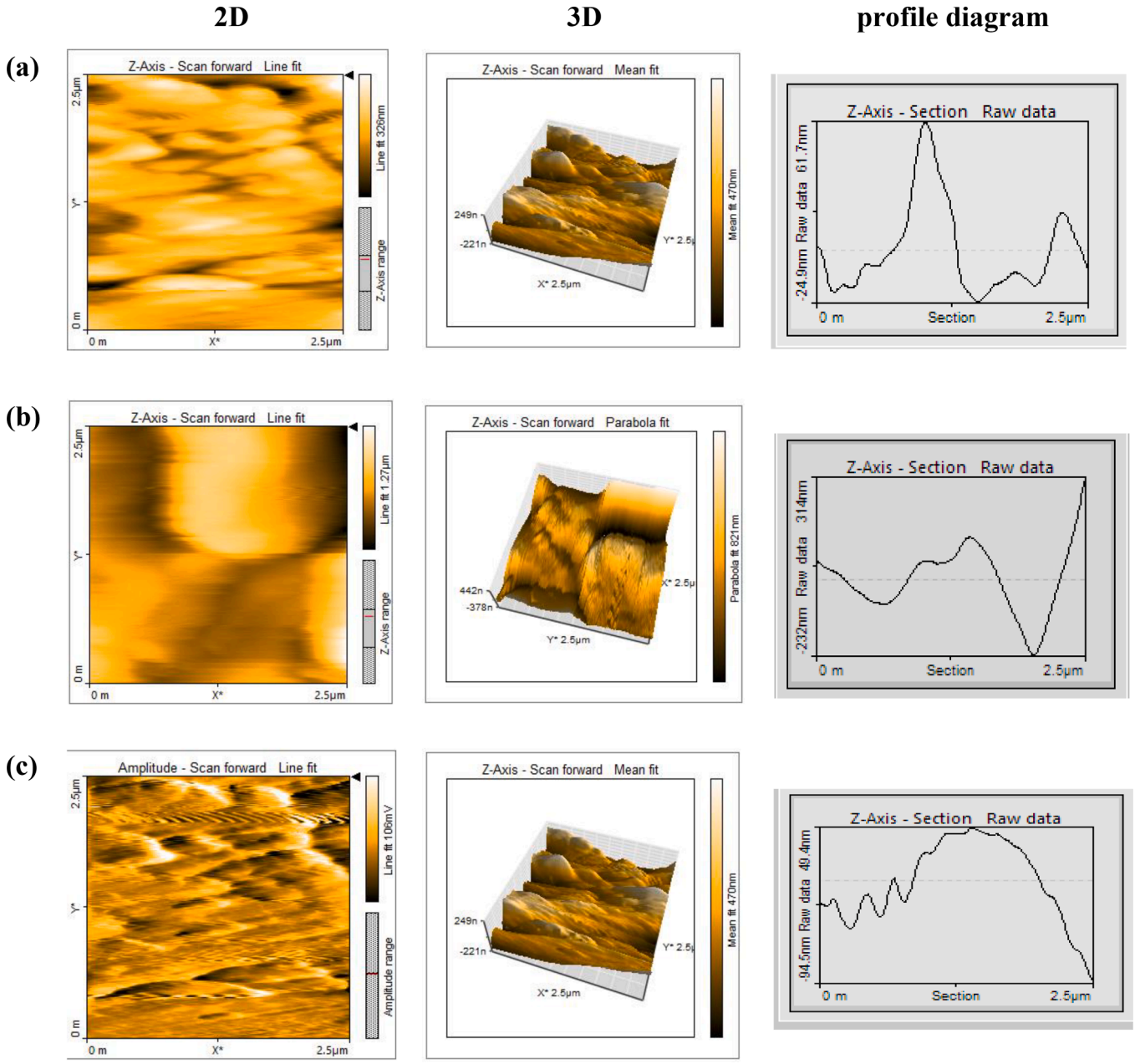

Fig. 10. AFM (2D&3D) images and corresponding profile diagram of of (free M.STL) surface (a), with in 0.5 M HCl solution only (b), and with addition of (**DICPT**) in test solution (c).

3.7. Theoretical analysis

The organic corrosion inhibitors can be devolped in corrosion field using a tool is called as computational chemical methods. In our study, we use DFT method to calculate the theoretical aspects of the inhibitor − metal interactions.

the optimized moleculer strcutre, molecular electron distribution (HOMO & LUMO), and molecular electrostatic potential (MESP) of (**DICPT**) are represnted in Fig. 11. It was found that, HOMO electron density localized on −C = O- of thiazole ring, acting as the initial electron donation center. While, LUMO electron density concentrated on −C-N-, −C-N- and −C = N- of pyrdine, acting as electron accepter center.

The reactive centers of (**DICPT**) molecules were confirmed from the (MESP) map obtained from analysis DFT.

As shown from (MESP) map (Fig. 11**d**)and corresponding charges of (**DICPT**) molucle in (Fig. 11e), The oxygen, nitorgon, thiohpene ring, and some phenyl carbons are the primary targets of the red to green region, which is related to electrophilic attack. The nucleophilic area, which is found across the whole (**DICPT**) moleuele, is related to the green to blue region. Generally, E_{HOMO} (Highest Occupied molecular Orbital) and E_{LUMO} (Lowest Unoccupied molecular Orbital) are are important descriptors obtained from the (DFT) analysis of (**DICPT**) molecules. These descriptors are crucial in understanding the electronic structure and properties of (**DICPT**) molecules,. Morever, E_{HOMO} represents the energy level of the highest occupied orbital in a molecule, indicating how easily an electron can be removed from the molecule, relating to its ionization potential. While, E_{LUMO} represents the energy level of the lowest unoccupied orbital, reflecting the molecule's ability to accept electrons, relating to its electron affinity.

The corresponding quantum chemical parameters of (**DICPT**) molecule derived from DFT calculatons were summerized in Fig. 12. These

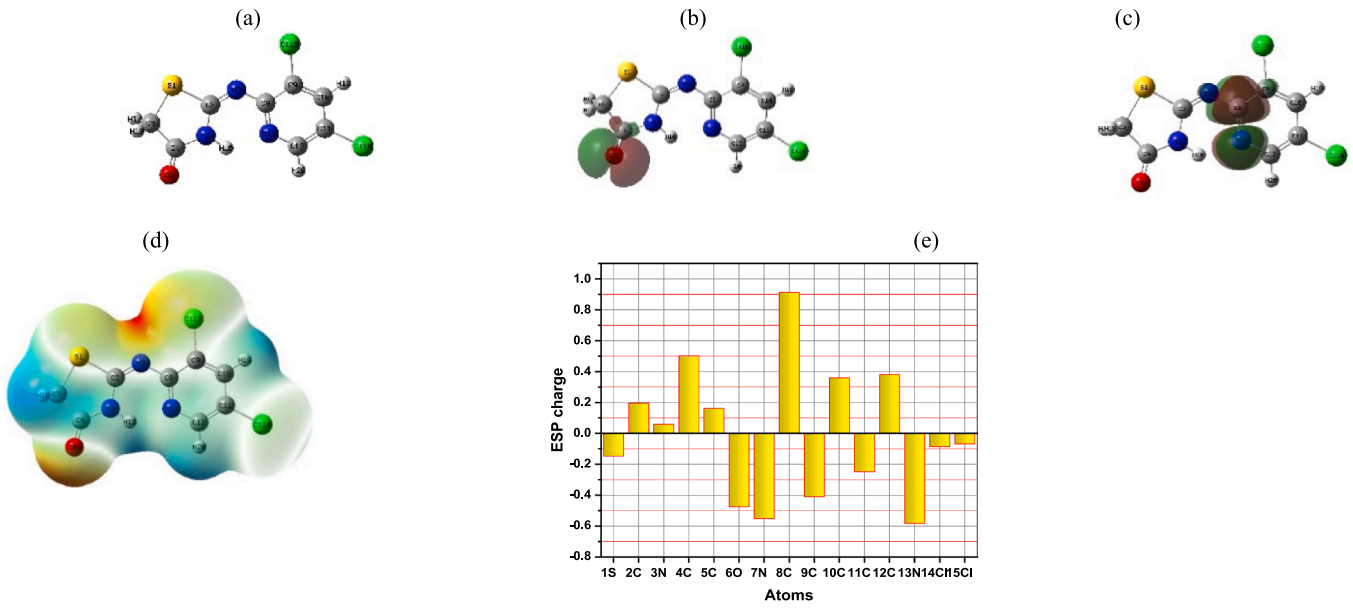

Fig. 11. Optimized moleculer strcutre (a), (HOMO and LUMO) distributions (b, c), molecular (MESP), and corrospending (MESP) plots (d, e) of (**DICPT**), respectively.

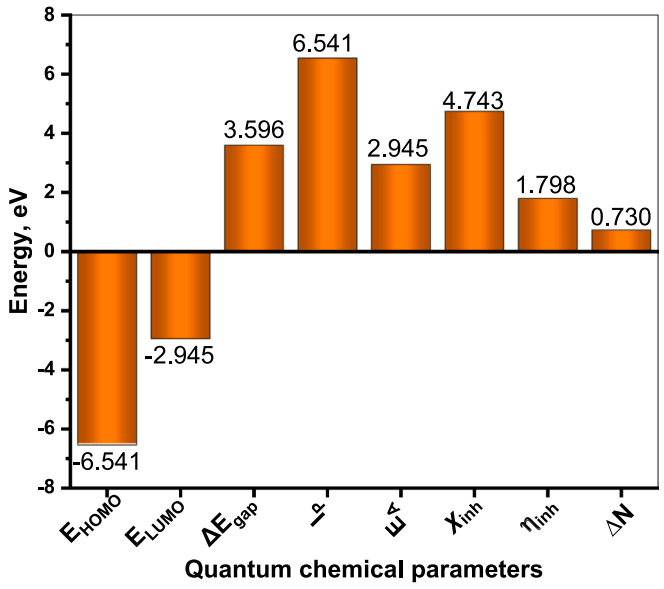

Fig. 12. Quantum chemical parameters of (**DICPT**).

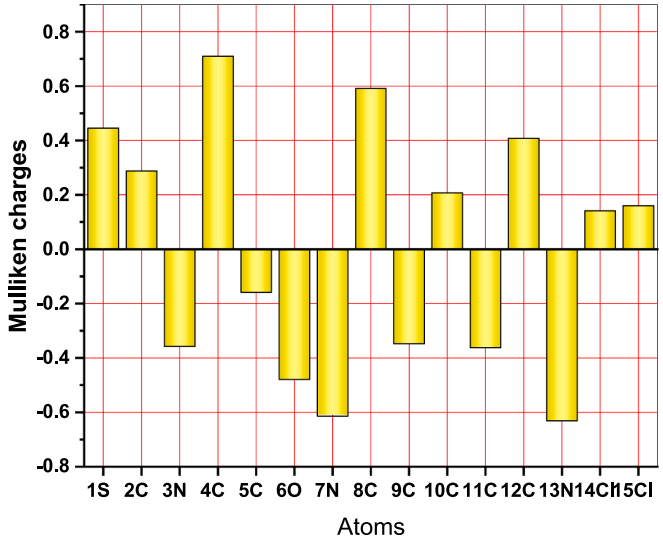

Fig. 13. Mulliken atomic charges of the (**DICPT**) molecule.

parameters were computed using the following equations (Jahdaly et al., 2022):

$$\Delta E_{gap} = E_{LUMO} - E_{HOMO} \quad (8)$$

$$I_P = -E_{HOMO} \quad (9)$$

$$E_A = -E_{LUMO} \quad (10)$$

$$\eta_{inh} = \frac{I_P - E_A}{2} \quad (11)$$

$$\chi_{inh} = \frac{I_P + E_A}{2} \quad (12)$$

$$\Delta N = \frac{(\varphi_{Fe} - x_{inh})}{2(\eta_{Fe} + \eta_{inh})} \quad (13)$$

where ΔE_{gap}, I_P, E_A, η_{inh}, χ_{inh}, ΔN and ϕ_{Fe} are energy gap between LUMO and HOMO ΔE_{gap}, the ionization potential (I_P), electron affinity (E_A), the absolute hardness (η_{inh}), the electronegativity (χ_{inh}), of inhibitor molecule, ΔN the fraction of electrons transferred and ϕ_{Fe} is the work function of Fe surface (4.82 eV), respectively.

As illustrated in Fig. 13, the high corrosion inhibition efficiency is provided by (**DICPT**) molecules with a reduced energy gap between LUMO and HOMO and a larger HOMO energy. Therefore, the larger HOMO energy and smaller energy gap between LUMO and HOMO energy can be responsible for the increased inhibitory efficiency of (**DICPT**) for M.STL corrosion in HCl solution (Jahdaly et al., 2022).

The interaction between inhibitor molecules and metal surface occurs, when the electron flow takes place from the inhibitor molecules which having smaller electronegativity to the metal which having larger electronegativity until the chemical potential between them becomes equal. The value of ΔN clarifies the number of electrons transferred from inhibitor molecules to the surface of metal. When, $\Delta N > 0$, the electron

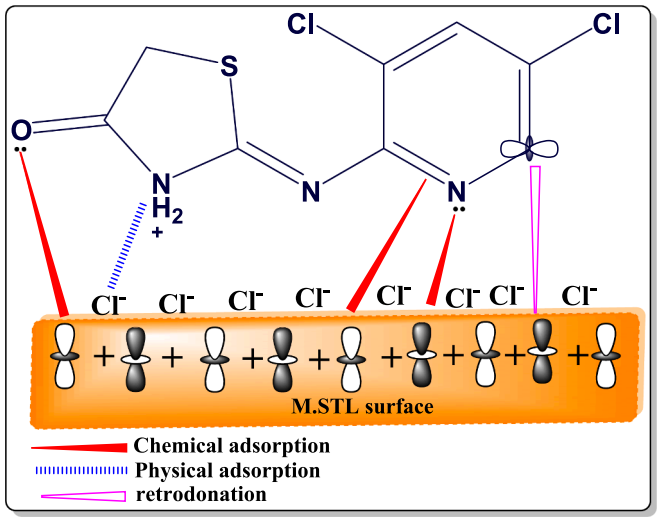

Fig. 14. Schematic illustration of adsorption mechanism of (**DICPT**) on M. STL surface.

transfer will occur from the inhibitor molecule to the metal surface. On the contrary, the electron transfer will occur from the metal surface to inhibitor molecule if $\Delta N < 0$ (Fouda et al., 2019). The value of $\Delta N > 0$ (Fig. 3), which point that the inhibitor molecules donate the electrons to M.STL surface. So, this outcome support the experimental protection efficiency.

The Mulliken atomic charges of the (**DICPT**) molecule are showed in Fig. 12, showing that, the heteroatoms have negative charges and are responsible for electrons donation to the unoccupied d-orbitals of the metal. while, the heteroatoms have positive charges and can accept electrons from the 3d orbital of the Fe atoms. Besides, the (6O, 7 N and 13 N) have a more negative charge, indicating that these atoms can take part in donor–acceptor interactions with surface metallic centers, thereby decreasing the corrosion rate on metal in the test solution (Fouda et al., 2019).

These theoretical findings via DFT analysis offer significant implications for corrosion inhibition, as they shed light on the inhibitor's ability to interact with the metal surface and mitigate corrosion processes. The correlations between DFT predictions and observed inhibition behavior underscore the importance of theoretical modeling in designing effective corrosion inhibitors.

3.8. Corrosion inhibition mechanism

Concepts from surface, DFT, and experimental data may be employed to clarify the (**DICPT**) inhibitor's adsorption mechanism on M.STL surface. As illustrated in Fig. 14, the (**DICPT**) molecule adsorbs on the M.STL surface by both physisorption and chemisorption moods based on PDP, EIS and the best fitting Langmuir absorption result.

In a 0.5 M HCl solution, the –NH- group of the (**DICPT**) molecule is protonated, which promotes the electrostatic interaction (physisorption) with negatively charged metal produced by reabsorbed Cl^- ions. Meanwhile, the accessible lone pair of electrons on heteroatoms (O, N) and π-electrons on the phenyl ring donate to the unoccupied 3d-orbitals of Fe, creating a chemisorption attraction (chemical adsorption) (Haque et al., 2018). Additionally, phenyl ring donation of π-electrons to vacant 3d orbitals of Fe and its vacant antibonding π-orbitals accepting electrons from filled metal orbitals at the same time provide the extra potential for the (**DICPT**) inhibitor to interact with mild steel (retrodonation) (Betti and Al-Amiery, 2023).

3.9. Comparison of (DICPT) performance with literature survey

Table 3 showcases the potential of (*Z*)-2-((3,5-dichloropyridin-2-yl) imino)thiazolidine-4-one (**DICPT**) as a corrosion inhibitor for mild steel in acidic media. While previously reported inhibitors (Ansari et al., 2016; Yadav et al., 2015; Kumar et al., 2013; Rbaa et al., 2020; Sharma et al., 2023; Yadav et al., 2015; Yadav et al., 2015) achieve similar or slightly higher protection efficiencies, **DICPT** achieves a remarkable 94.4 % inhibition at a lower concentration (30 ppm) in 0.5 M HCl. This suggests it might be more efficient in terms of inhibitor usage. However, further investigation is needed. Evaluating **DICPT's** performance at harsher acid concentrations and understanding its inhibition mechanism (film formation, ion scavenging, etc.) would provide a more complete picture. Additionally, exploring synergistic effects with other inhibitors and assessing the cost, availability, and environmental impact of **DICPT** are crucial for its practical application. By addressing these aspects, researchers can solidify **DICPT's** position as a promising candidate for

Table 3
The compression of the %I of (**DICPT**) with previous some organic inhibitors.

Inhibitor	Metal/acid conc	experimental methods	Adsorption isotherm	ΔG°_{ads}	Conc/% I	References
2–4(di-1Hindole-3-yl-3-azabicyspiro-4-acetyl-2-acetylamino −1,3,4-thiadiazoline (DIAT)	N80 steel/ 15 % HCl	WL, PDP, EIS, SEM	Langmuir	−34.1	50 ppm/ 97.05	(Ansari et al., 2016)
(Z)-5-(4-methoxybenzylidene)-3-(benzo[d]thiazol2-yl)-2-(4-methoxyphenyl) thiazolidine-4-one	Mild steel/ 15 % HCl	WL, PDP, EIS SEM and EDX, AFM	Langmuir	−42.5	50 ppm/ 91.2	(Yadav et al., 2015)
2,4-bis (methoxyphenyl)- 1H-benzodiazepine	N80 steel/ 15 % HCl	WL, PDP, EIS, SEM	Langmuir	−37.8	200 ppm/ 93.0	(Kumar et al., 2013)
5-((2-aminoethoxy) methyl) quinolin-8-ol	Mild steel/ 1.0 M HCl	WL, PDP, EIS, SEM	Langmuir	−37.5	218 ppm/ 98.2	(Rbaa et al., 2020)
4–((4–bromo-2–hydroxybenzylidene)amino)–1,5–dimethyl–2–phenyl–1H–pyrazole–3(2H)-one (BHAP)	Mild steel/ 1.0 M HCl	PDP, EIS, UV FTIR, SEM, EDX	Langmuir	−41.9	200 ppm/ 93.9	(Sharma et al., 2023)
5-[2-(3,4,5-trimethoxyphenyl)-6-(4-methoxylphenyl)-imidazo[2,1-b] (Öztürk, 2017; Hegazy et al., 2015; El-Haddad and Fouda, 2015) thiadiazol-5-yl) methylidene]-1,3-thiazolidine-2,4-dione	Mild steel/ 15 % HCl	WL, PDP, EIS, SEM	Langmuir	−37.8	200 ppm/ 93.1	(Yadav et al., 2015)
3-(4-(1-acetyl-5-(4-meth-oxyphenyl)-4,5-dihydro-1H-pyrazol-3-yl) phenyl) spiro [indoline-3,2- thiazolidine]-2,4-dione	N80 steel/ 15 % HCl	WL, PDP, EIS, SEM, AFM	Langmuir	−37.4	200 ppm/ 92.0	(Yadav et al., 2015)
(Z)-2-((3,5-dichloropyridin-2-yl)imino)thiazolidine −4-one (**DICPT**)	Mild steel/ 0.5 MHCl	PDP, EIS, UV, AFM	Langmuir	−34.1	30 ppm/ 94.4	Our compound

protecting mild steel from acidic corrosion.

4. Conclusions

In our investigation, we thoroughly examined the corrosion inhibition capabilities of (**DICPT**) for M.STL in a the 0.5 M HCl solution, employing a combination of experimental and theoretical methodologies.

Our experimental findings underscore the remarkable corrosion inhibiting properties of **DICPT**. Through polarization studies, we observed that **DICPT** operates as a mixed-type inhibitor, effectively impeding both anodic and cathodic corrosion processes. This inhibition mechanism was further supported by our analysis based on the Langmuir adsorption isotherm, which revealed strong adsorption of **DICPT** molecules onto the mild steel surface, forming a protective barrier against corrosion.

Additionally, our experimental results were complemented by UV–visible spectrometry and Atomic Force Microscopy (AFM) analyses, which provided visual confirmation of **DICPT** adsorption on the M.STL surface. These analyses not only corroborated our electrochemical findings but also offered insights into the morphological and optical changes induced by DICPT, indicative of its corrosion-inhibiting effect.

Furthermore, our theoretical investigations, conducted using Density Functional Theory (DFT) calculations, yielded valuable insights into the molecular-level interactions between DICPT and mild steel. These calculations provided a detailed understanding of the reactivity of **DICPT** molecules with the metal surface, which aligned closely with our experimental observations.

CRediT authorship contribution statement

Ghada S. Masaret: Writing – review & editing, Writing – original draft, Investigation, Funding acquisition, Formal analysis. **Reem Shah:** Visualization, Software, Methodology.

Declaration of competing interest

The authors declare that they have no known competing financial interests or personal relationships that could have appeared to influence the work reported in this paper.

Acknowledgement

The authors would like to thank *Umm Al-Qura University*, *Saudi Arabia,* for their excellent technical assistance during the work.

Appendix A. Supplementary data

Table S1, Fig. S1. The ^{13}C −NMR (DMSO-d_6) spectrum of (**DICPT**), Fig. S2. The mass spectrum of inhibitor (**DICPT**). Supplementary data to this article can be found online at https://doi.org/10.1016/j.arabjc.2024.105807.

References

Abdelaziz, S., Benamira, M., Messaadia, L., Boughoues, Y., Lahmar, H., Boudjerda, A., 2021. Green corrosion inhibition of mild steel in HCl medium using leaves extract of Arbutus unedo L. plant: An experimental and computational approach. Colloids Surf A Physicochem Eng Asp 619, 126496.

Abdel-Rehim, S.S., Khaled, K.F., Abd-Elshafi, N.S., 2006. Electrochemical frequency modulation as a new technique for monitoring corrosion inhibition of iron in acid media by new thiourea derivative. Electrochim. Acta 51 (16), 3269–3277.

Abdou, M.M., El-Haddad, M.N., 2022. Synthesis of tolyl guanidine as copper corrosion inhibitor with a complementary study on electrochemical and in silico evaluation. Sci. Rep. 12 (1), 14893.

Adjimani, J.P., Asare, P., 2015. Antioxidant and free radical scavenging activity of iron chelators. Toxicol. Rep. 2, 721–728.

Alamry, K.A., Aslam, R., Khan, A., Hussein, M.A., Tashkandi, N.d.Y., 2022. Evaluation of corrosion inhibition performance of thiazolidine-2, 4-diones and its amino derivative: Gravimetric, electrochemical, spectroscopic, and surface morphological studies. Process Saf. Environ. Prot. 159, 178–197.

Alhaffar, M.T., Umoren, S.A., Obot, I.B., Ali, S.A., 2018. Isoxazolidine derivatives as corrosion inhibitors for low carbon steel in HCl solution: experimental, theoretical and effect of KI studies. RSC Adv. 8 (4), 1764–1777.

Al-nami, S.Y., Aljuhani, E., Althagafi, I., Abumelha, H.M., Bawazeer, T.M., Al-Solimy, A. M., Al-Ahmed, Z.A., Al-Zahrani, F., El-Metwaly, N., 2021. Synthesis and Characterization for new nanometer Cu (II) complexes, conformational study and molecular docking approach compatible with promising in vitro screening. Arab. J. Sci. Eng. 46, 365–382.

Ansari, K.R., Sowmya Ramkumar, Nalini, D., Quraishi, M.A., 2016. Studies on adsorption and corrosion inhibitive properties of quinoline derivatives on N80 steel in 15% hydrochloric acid. Cogent Chem. 2 (1), 1145032.

Apotrosoaei, M., Vasincu, I., Sandra Constantin, F., Buron, S.R., Profire, L., 2014. Synthesis, characterization and antioxidant activity of some new thiazolidin-4-one derivatives. Med.-Surg. J. 118 (1), 213–218.

Balachandar, S., Dhandapani, Munusamy, Israel Vijayan Muthu Vijayan Enoch, Suganthi, Soundrapandian, 2017. Structural analysis, molecular docking and DFT calculations of Bis (Pyrazolium Picrate) monohydrate interaction with calf thymus DNA and microbes. ChemistrySelect 2 (29), 9298–9311.

Bandeira, Marinho, Rafael, van Drunen, Julia, Tremiliosi-Filho, Germano, Jose Ribeiro dos Santos Junior, Elias, José Milton, de Matos, 2017. Polyaniline/polyvinyl chloride blended coatings for the corrosion protection of carbon steel. Progress in Organic Coatings 106, 50–59.

Benali, O., 2015. Corrosion inhibition of mild steel in acidic media using newly synthesized heterocyclic organic molecules: Correlation between inhibition efficiency and chemical structure. AIP Conf. Proc. 1653 (1).

Betti, N., Al-Amiery, A.A., Al-Azzawi, Waleed Khalid, Isahak, Wan Nor Roslam Wan, 2023. Corrosion inhibition properties of schiff base derivative against mild steel in HCl environment complemented with DFT investigations. Sci. Rep. 13 (1), 8979.

Boudjellal, F., Ouici, H.B., Guendouzi, A., Benali, O., Sehmi, A., 2020. Experimental and theoretical approach to the corrosion inhibition of mild steel in acid medium by a newly synthesized pyrazole carbothioamide heterocycle. J. Mol. Struct. 1199, 127051.

Brahmbhatt, H., Molnar, M., Pavić, V., Rastija, V., 2019. Synthesis, characterization, antibacterial and antioxidant potency of N-substituted-2-sulfanylidene-1, 3-thiazolidin-4-one derivatives and QSAR study. Med. Chem. 15 (8), 840–849.

Capaldo, L., Ravelli, D., 2017. Hydrogen atom transfer (HAT): a versatile strategy for substrate activation in photocatalyzed organic synthesis. Eur. J. Org. Chem. 2017 (15), 2056–2071.

Chen, H., Hebo Ye, Yu., Hai, L.Z., You, L., 2020. n→ π* interactions as a versatile tool for controlling dynamic imine chemistry in both organic and aqueous media. Chem. Sci. 11 (10), 2707–2715.

Deep, Aakash, Balasubrmanian Narasimhan, Lim, Siong Meng, Ramasamy, Kalavathy, Mishra, Rakesh Kumar, Mani, Vasudevan, 2016. 4-Thiazolidinone derivatives: synthesis, antimicrobial, anticancer evaluation and QSAR studies. RSC Adv. 6 (111), 109485–109494.

Dohare, P., Chauhan, D.S., Sorour, A.A., Quraishi, M.A., 2017. DFT and experimental studies on the inhibition potentials of expired Tramadol drug on mild steel corrosion in hydrochloric acid. Mater. Discover 9, 30–41.

El Haddad Mahmoud, N., Salem, Aya M., Wahba, Ahmed M., El Maksous Samir Abd, A., 2023. Experimental and theoretical optimization of Chelidonium Majus (Papaveraceae) extract as an environmentally friendly inhibitor for corrosion of a-brass in nitric acid solution. Mater. Protect. 64 (3), 239–255.

El-Haddad, M.N., 2020. Spectroscopic, electrochemical and quantum chemical studies for adsorption action of polyethylene oxide on copper surface in NaCl solution. Z. Phys. Chem. 234 (11–12), 1835–1851.

El-Haddad, M.N., Abd, E.-A., Fouda,, 2021. Evaluation of curam drug as an ecofriendly corrosion inhibitor for protection of stainless steel-304 in hydrochloric acid solution: chemical, electrochemical, and surface morphology studies. J. Chin. Chem. Soc. 68 (5), 826–836.

El-Haddad, M.N., Abd, E.-A., Fouda., 2013. Corrosion inhibition effect and adsorption of aniline derivatives on QD36 steel surface in acidic solution. Prot. Met. Phys. Chem 49, 753–762.

El-Haddad, M.N., Elattar, K.M., 2013. Role of novel oxazocine derivative as corrosion inhibitor for 304 stainless steel in acidic chloride pickling solutions. Res. Chem. Intermed. 39, 3135–3149.

El-Haddad, M.N., Fouda, A.S., 2013. Corrosion inhibition and adsorption behavior of some azo dye derivatives on carbon steel in acidic medium: synergistic effect of halide ions. Chem. Eng. Commun. 200 (10), 1366–1393.

El-Haddad, M.N., Fouda, A.S., 2015. Electroanalytical, quantum and surface characterization studies on imidazole derivatives as corrosion inhibitors for aluminum in acidic media. J. Mol. Liq. 209, 480–486.

Foti, M.C., 2015. Use and Abuse of the DPPH• Radical. J. Agric. Food Chem. 63 (40), 8765–8776.

Fouda, A.S., Badr, G.E., El-Haddad, M.N., 2008. The Inhibition of C-steel Corrosion in H_3PO_4 Solution by Some Furfural Hydrazone Derivatives. J. Korean Chem. Soc. 52 (2), 124–132.

Fouda, A.S., El-Haddad, M.N., Ismail, M.A., Abd Elgyed, A., 2019. Investigation of 6-[5-(4-Methoxyphenyl) furan-2-yl] nicotinonitrile as a new corrosion inhibitor for carbon steel in acidic solution: Chemical, electrochemical and quantum chemical studies. J. Bio-and Tribo-Corr. 5, 1–14.

Gerengi, H., Solomon, M.M., Öztürk, S., Yıldırım, A., Gece, G., Kaya, E., 2018. Evaluation of the corrosion inhibiting efficacy of a newly synthesized nitrone against St37 steel corrosion in acidic medium: experimental and theoretical approaches. Mater. Sci. Eng. C 93, 539–553.

Haque, J., Verma, C., Vandana Srivastava, M.A., Quraishi, and Eno E. Ebenso., 2018. Experimental and quantum chemical studies of functionalized tetrahydropyridines as corrosion inhibitors for mild steel in 1 M hydrochloric acid. Results Phys. 9, 1481–1493.

Hegazy, M.A., Abd El Rehim, S.S., Badawi, A.M., Ahmed, M.Y., 2015. Studying the corrosion inhibition of carbon steel in hydrochloric acid solution by 1-dodecyl-methyl-1 H-benzo [d][1, 2, 3] triazole-1-ium bromide. RSC Adv. 5 (61), 49070–49079.

Hilbert, L.R., Bagge-Ravn, D., Kold, J., Gram, L., 2003. Influence of surface roughness of stainless steel on microbial adhesion and corrosion resistance. Int. Biodeter. Biodegr. 52 (3), 175–185.

Hu, K.e., Zhuang, J., Ding, J., Ma, Z.u., Wang, F., Zeng, X., 2017. Influence of biomacromolecule DNA corrosion inhibitor on carbon steel. Corros. Sci. 125, 68–76.

Isloor, A.M., Sunil, D., Shetty, P., Shridhar Malladi, Pai, K.S.R., Maliyakkl, Naseer, 2013. Synthesis, characterization, anticancer, and antioxidant activity of some new thiazolidin-4-ones in MCF-7 cells. Med. Chem. Res. 22, 758–767.

Ismail, M.A., Shaban, M.M., Abdel-Latif, E., Abdelhamed, F.H., Migahed, M.A., El-Haddad, M.N., Abousalem, A.S., 2022. Novel cationic aryl bithiophene/terthiophene derivatives as corrosion inhibitors by chemical, electrochemical and surface investigations. Sci. Rep. 12 (1), 3192.

Jahdaly, A.l., Badreah, A., 2023. Evaluation of adsorption and inhibitive properties of Capparis spinoza leaves extract on high carbon steel corrosion in acidic media. Chem. Pap. 77 (11), 6605–6612.

Jahdaly, A.l., Badriah, A., Masaret, G.A.S., 2022. Synthesis and inhibitive behavior of new thiazolyl-pyrazole derivative at low carbon steel/HCl interface: Electrochemical, morphology and theoretical investigations. J. Mol. Liq. 364, 119933.

Kaya, Savaş, Lgaz, Hassane, Thakkur, Abhinay, Kumar, Ashish, Işın, Dilara Özbakır, Karakuş, Nihat, Ahmed, Samia Ben, 2023. Molecular insights into the corrosion inhibition mechanism of omeprazole and tinidazole: a theoretical investigation. Mol. Simulation 49 (17), 1632–1646.

Keshk, A.A., Fouda, A.S., 2014. Some thiazolodine-5-one derivatives as corrosion inhibitors for carbon steel in 2 M HCl solutions. Int. J. Adv. Res. 2 (3), 737–750.

Kitts, D.D., Wijewickreme, A.N., Chun, Hu., 2000. Antioxidant properties of a North American ginseng extract. Mol. Cell. Biochem. 203, 1–10.

Kumar, S., Sharma, D., Yadav, P., Yadav, M., 2013. Experimental and quantum chemical studies on corrosion inhibition effect of synthesized organic compounds on N80 steel in hydrochloric acid. Ind. Eng. Chem. Res. 52 (39), 14019–14029.

Lgaz, H., Saha, S.K., Abdelkarim Chaouiki, K., Bhat, S., Salghi, R., Banerjee, P., Ali, I.H., Khan, M.I., Chung, I.-M., 2020. Exploring the potential role of pyrazoline derivatives in corrosion inhibition of mild steel in hydrochloric acid solution: Insights from experimental and computational studies. Constr. Build. Mater. 233, 117320.

Lgaz, Hassane, Saha, Sourav Kr, Lee, Han-seung, Kang, Namhyun, Thari, Fatima Zahra, Karrouchi, Khalid, Salghi, Rachid, Bougrin, Khalid, Ali, Ismat Hassan, 2021. Corrosion inhibition properties of thiazolidinedione derivatives for copper in 3.5 wt. % NaCl medium. Metals 11 (11), 1861.

Masaret, G.A.S., Al, B.A., Jahdaly., 2021. Inhibitive and adsorption behavior of new thiazoldinone derivative as a corrosion inhibitor at mild steel/electrolyte interface: Experimental and theoretical studies. J. Mol. Liq. 338, 116534.

Masroor, S., Mobin, M., Alam, M.J., Ahmad, S., 2017. The novel iminium surfactant p-benzylidene benzyldodecyl iminium chloride as a corrosion inhibitor for plain carbon steel in 1 M HCl: electrochemical and DFT evaluation. RSC Adv. 7 (37), 23182–23196.

Nezhawy, E.l., Ahmed, O.H., Ramla, M.M., Khalifa, N.M., Abdulla, M.M., 2009. Synthesis and antioxidant activity of some thiazolidin-4-one derivatives. Monatshefte Für Chemie-Chemical Monthly 140, 531–539.

Ouici, H.B., Benali, O., Harek, Y., Larabi, L., Hammouti, B., Guendouzi, A., 2013. Inhibition of mild steel corrosion in 5% HCl solution by 5-(2-hydroxyphenyl)-1, 2, 4-triazole-3-thione. Res. Chem. Intermed. 39, 2777–2793.

Öztürk, S., 2017. Synthesis and corrosion inhibition effects of quinazolin-(3H)-4-one derivatives containing long-chain pyridinium salts on carbon steel in 1.5 M HCl. Prot. Met. Phys. Chem 53, 920–927.

Patel, D., Kumari, P., Patel, N., 2012. Synthesis and biological evaluation of some thiazolidinones as antimicrobial agents. Eur. J. Med. Chem. 48, 354–362.

Plesniak, M.P., Huang, H.-M., Procter, D.J., 2017. Radical cascade reactions triggered by single electron transfer. Nat. Rev. Chem. 1 (10), 0077.

Rao, BV.A., Iqbal, M.Y., Sreedhar, B., 2009. Self-assembled monolayer of 2-(octadecylthio) benzothiazole for corrosion protection of copper. Corros. Sci. 51 (6), 1441–1452.

Rbaa, M., Benhiba, F., Abousalem, A.S., Galai, M., Rouifi, Z., Oudda, H., Lakhrissi, B., Warad, I., Zarrouk, A., 2020. Sample synthesis, characterization, experimental and theoretical study of the inhibitory power of new 8-hydroxyquinoline derivatives for mild steel in 1.0 M HCl. J. Mol. Struct. 1213, 128155.

Sehmi, A., Ouici, H.B., Guendouzi, A., Ferhat, M., Benali, O., Boudjellal, F.J.J.S., 2020. Corrosion inhibition of mild steel by newly synthesized pyrazole carboxamide derivatives in HCl acid medium: Experimental and theoretical studies. J. Electrochem. Soc. 167 (15), 155508.

Sharma, D., Thakur, A., Sharma, M.K., Sharma, R., Suresh Kumar,Ashish Sihmar, Hariom Dahiya,, et al., 2023. Effective corrosion inhibition of mild steel using novel 1, 3, 4-oxadiazole-pyridine hybrids: Synthesis, electrochemical, morphological, and computational insights. Environ. Res. 234, 116555.

Sharma, D., Thakur, A., Sharma, M.K., Kumar, A., Jakhar, K., Suresh Kumar,Ashish Sihmar,, et al., 2023. A convenient synthesis, electrochemical profiling, and morphological studies of a pyridine-based 1, 3, 4-oxadiazole hybrid: A promising study for corrosion mitigation of mild steel in strongly acidic environment. Inorg. Chem. Commun. 158, 111554.

Sharma, Manish, Yadav, Satendra Singh, Sharma, Priya, Lalita Yadav, Md, Abedeen, Zainul, Kushwaha, Himmat Singh, Gupta, Ragini, 2023. An experimental and theoretical investigation of corrosion inhibitive behaviour of 4-amino antipyrine and its Schiff`s base (BHAP) on mild steel in 1 M HCl solution. Inorg. Chem. Commun. 157, 111330.

Singh, A., Ansari, K.R., Ali, I.H., Ibrahimi, B.EL., Sharma, N.R., Bansal, A., Alanazi, A.K., Younas, M., Alamri, A.H., Lin, Y., 2023. Heteroatomic organic compound as a novel corrosion inhibitor for carbon steel in sulfuric acid: Detail experimental, surface, molecular docking and computational studies. Colloids Surf A Physicochem Eng Asp 673, 131692.

Thakur, Abhinay, Dagdag, O., Berisha, Avni, Ebenso, Eno E., Kumar, Ashish, Sharma, Shveta, Ganjoo, Richika, Assad, Humira, 2024. Mechanistic insights into the corrosion inhibition of mild steel by eco-benign Asphodelus Tenuifolius aerial extract in acidic environment: Electrochemical and computational analysis. Surface Coat. Technol. 130568.

Thakur, A., Kumar, A., Kaya, S., Benhiba, F., Sharma, S., Ganjoo, R., Assad, H., 2023. Electrochemical and computational investigations of the Thysanolaena latifolia leaves extract: An eco-benign solution for the corrosion mitigation of mild steel. Results in Chemistry 6, 101147.

Wang, S., Zhao, Y., Zhang, G., Lv, Y., Zhang, N., Gong, P., 2011. Design, synthesis and biological evaluation of novel 4-thiazolidinones containing indolin-2-one moiety as potential antitumor agent. Eur. J. Med. Chem. 46 (8), 3509–3518.

Yadav, M., Behera, D., Kumar, S., Yadav, P., 2015. Experimental and quantum chemical studies on corrosion inhibition performance of thiazolidinedione derivatives for mild steel in hydrochloric acid solution. Chem. Eng. Commun. 202 (3), 303–315.

Yadav, M., Kumar, S., Kumari, N., Bahadur, I., Ebenso, E.E., 2015. Experimental and theoretical studies on corrosion inhibition effect of synthesized benzothiazole derivatives on mild steel in 15% HCl solution. Int. J. Electrochem. Sci. 10 (1), 602–624.

Yadav, M., Sarkar, T.K., Purkait, T., 2015. Studies on adsorption and corrosion inhibitive properties of indoline compounds on N80 steel in hydrochloric acid. J. Mater. Eng. Perform. 24, 4975–4984.